Chapter 1

Introduction and Literature Survey

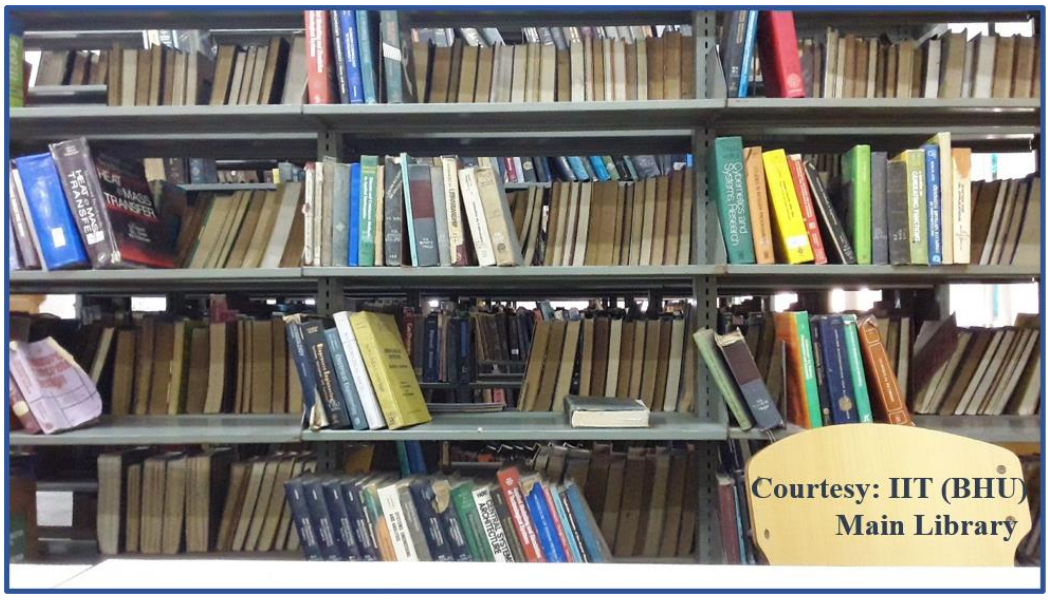

This chapter deals with the concise introduction about the materials, we opted for our research study and its related properties. It also elaborates the general theory related to the electrochemical and photochemical applications. It ends with short descriptions about the available scope and motivation for the research work.

1.1 g-C_3N_4: Brief Historical Background and Synthesis Process

Carbon nitride (C_3N_4) is privileged to be in the class of the oldest synthetic polymers, known to the scientific community. Jöns Jakob Berzelius is credited for the discovery of carbon nitride in form of Heptazine (tri-s-triazine; three fused triazine rings) synthesized by ignition of mercury thiocyanate in 1830. When heptazine units are polymerized with help of amine linkage (—NH—), the structure obtained is called 'melon' $(C_6N_9H_3)_n$ termed used by Justus von Liebig in 1834 (*see* Fig. 1.1; Heptazine and Melon). [1,2] Liebig prepared melon by reaction of chlorine with potassium thiocyanate solution. The chemical formula of melon was first mentioned by Franklin as $H_3C_6N_9$ in 1922, along with a description of how it is obtained from various nitrogen-containing sources such as guanidine, biguanide, cyanamide, dicyandiamide and melamine under the description of "THE AMMONO CARBONIC ACIDS". [3] Graphitic carbon nitride is pronounced to be the oldest synthetic polymer, yet the complete polymeric structure was not known till 2001 owing to its inertness and low solubility of intermediaries. [4-8]

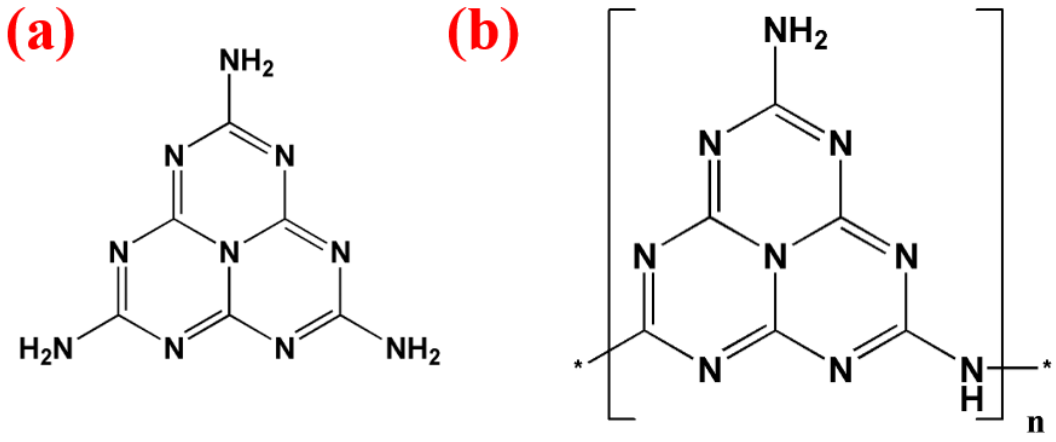

Fig. 1.1 (a) Heptazine (tri-s-triazine) and (b) Melon $(C_6N_9H_3)n$.

Seven allotropes of C_3N_4 have been reported α-C_3N_4, β-C_3N_4, g-h-triazine, g-h-heptazine, g-o-triazine, cubic and pseudocubic-C_3N_4, among them graphitic phase of carbon nitride viz. g-C_3N_4 made up of tri-s-triazine units (heptazine; C_6N_7) is most stable (by 30 kJ mol^{-1}) under ambient condition owing to the electronic surroundings around N atom and size of nitride pores. [4] Both triazine (C_3N_4) and tri-s-triazine (C_6N_7) acts as basic units to make the potential allotropes of g-C_3N_4 (*see* Fig. 1.2), although differ in the stability owing to the electronic environment around the N atom and size of the nitride pores. Its graphitic structure arises from the tri-s-triazine units connected by the planar amino groups.

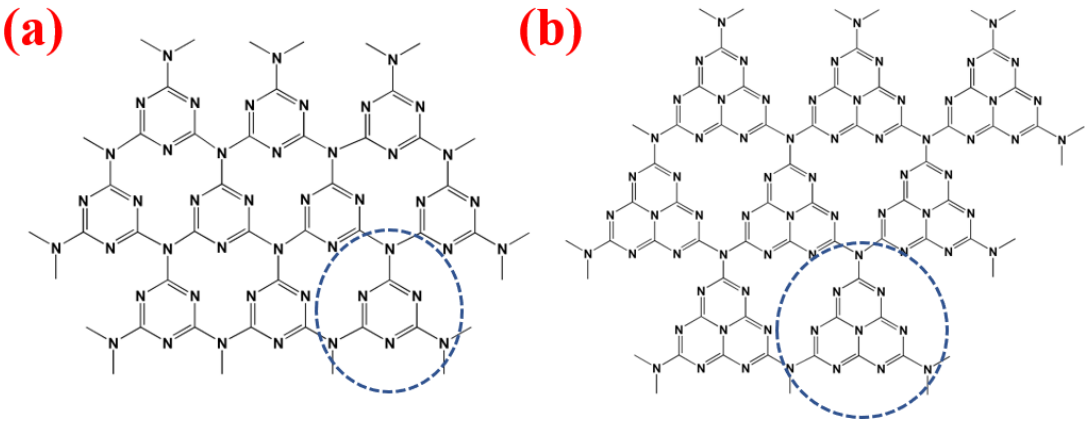

Fig. 1.2 (a) triazine and (b) tri-s-triazine (heptazine) based g-C_3N_4. The circled part shows the repeating unit of the respective structures.

The g-C_3N_4 based on the tri-s-triazine units is synthesized via thermal polymerization of a range of easily available N-rich precursors viz. Urea, Thiourea,

Cyanamide, Dicyandiamide, Melamine as shown in Figure 1.3 (a). [9] Its polymerization process involves the combination of polyaddition and polycondensation schemes. The synthesis pathway from precursor to final 2D carbon nitride polymer proceeds from several intermediate structures ultimately culminating into a graphitic structure. Figure 1.3 (b) represents the simplified synthetic pathway for the carbon nitride polymer. [5]

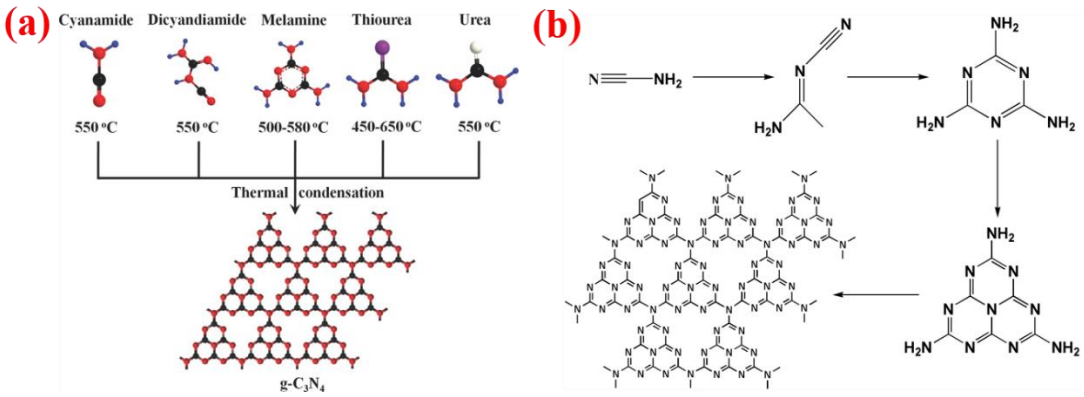

Fig. 1.3 (a) Various Precursors for the synthesis of g-C_3N_4. The colour code in the structures: black for C; red for N; blue for H; purple for S; white for O. Reprinted with permission from ref. [9] (License No. 5200050596511) Copyright@2015*WILEY*; 1.3 (b) Reaction pathway for the synthesis of graphitic carbon nitride.

Dicyandiamide, Melamine as well as Urea, and Thiourea are the most used commercial precursors to synthesize bulk g-C_3N_4. The precursors (cyanamide and dicyandiamide) first condense to make melamine at the temperature of ~240 ºC. Melamine remains the major product till 350 ºC, from this onwards rearrangement of

melamine results into tri-s-triazine units via Melam (ditriazinylamine) at around 390 ºC. It involves the elimination of NH_3. Condensation of tri-s-triazine units led to various intermediate units termed such as melem, dimelem and melon described in detail further, ultimately condensing to bulk g-C_3N_4 at 520 ºC. g-C_3N_4 is the final de-amination product obtained by a series of intermediaries, but at a higher temperature (>650 ºC), it undergoes complete decomposition instead of losing ammonia. [6]

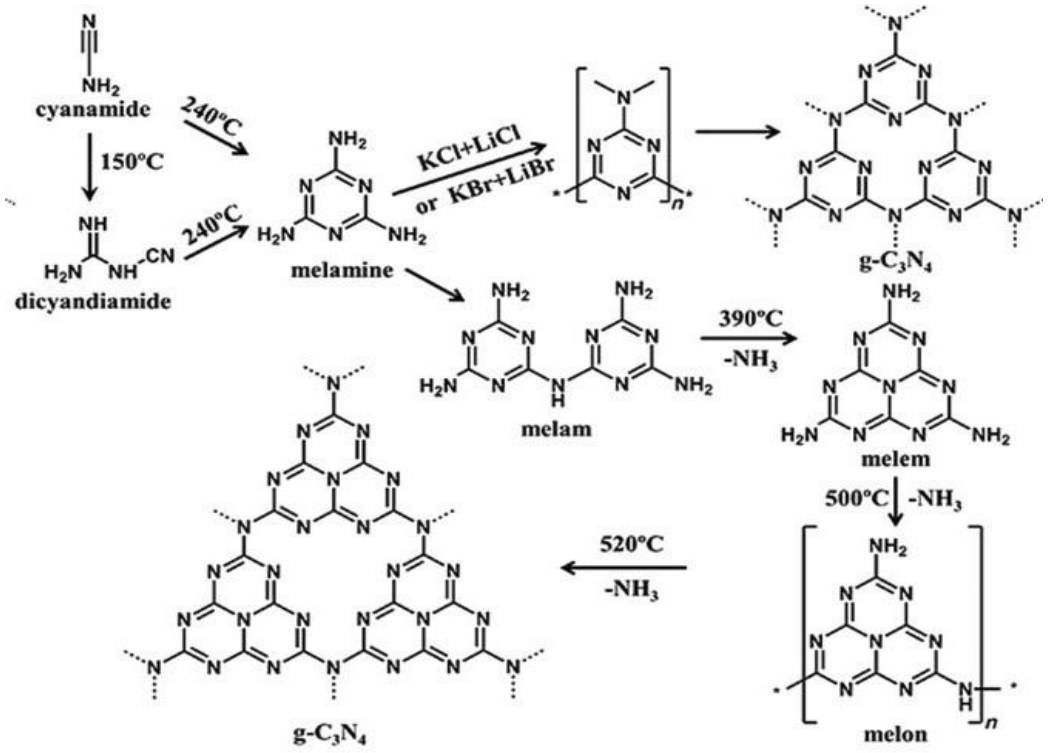

Fig. 1.4 Two different reaction pathways for the synthesis of triazine-based graphitic carbon nitride and tri-s-triazine based graphitic carbon nitride. Reprinted with permission from Ref. [14] (License No. 5204721397545) Copyright@2015*WILEY*.

Several efforts have been made to chalk out the condensation process of melamine, elemental composition and structure of intermediaries since their early discovery, but chemical inertness and poor solubility of condensation products hinder their characterization. In 1959, H. May reported the formation of melam, melem and melon upon pyrolysis of Melamine at a temperature range of 200-500 °C by elemental analysis. [7] Two routes were proposed leading to the structural elucidation of g-C_3N_4. In one of the proposed routes, Melamine also referred to as a trimer of cyanamide, at first condenses to Melam: $(H_2N)_2(C_3N_3)NH(C_3N_3)(NH_2)_2$, formed by linking of two molecules of melamine losing one ammonia (Melamine: ammonia = 2:1). [5] Melam is a ditriazinylamine structure proposed by Klason as early as 1886. [10] Tautomeric form of melam has also been proposed resonating between two triazine rings as shown in Figure 1.5. [5] Substituted Melam prepared by fusion of chloro-s-triazines and amino-s-triazines derivatives have also been reported in 1962 by Wilhelm J. Schnabel et al. It confirmed the synthesis of tri-s-triazine nuclei as derivative of melam. [8]

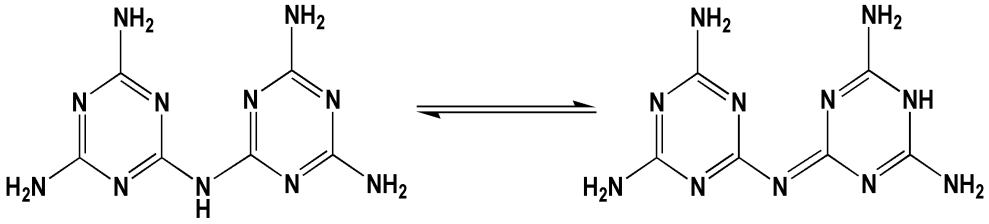

Fig. 1.5 Proposed Tautomeric forms of melam. [5]

Melam further condensates into melem: (2,5,8-triamino-tri-s-triazine) $C_6N_7(NH_2)_3$ which is a repeating unit of g-C_3N_4, liberating ammonia (Melam to ammonia 1:1). This melem dimerizes into di-melem which forms polymeric melon sheets: $(C_6N_9H_3)_n$, which on further liberation of Ammonia gives graphitic structure. Figure 1.4 displays the reaction pathway along with the synthesis of triazine-based g-C_3N_4. In another proposed route, melem: $C_6N_7(NH_2)_3$ is the first condensation product of Melamine (Melamine: ammonia = 1:1), further condensation gives melon followed by graphitic carbon nitride (g-C_3N_4) with the liberation of ammonia. Although, this route is less accepted as conformation of intermediatory melon is still awaited among scientific peers. The energy per atom of different intermediaries is shown in the energy diagram as shown in Figure 1.6. [11]

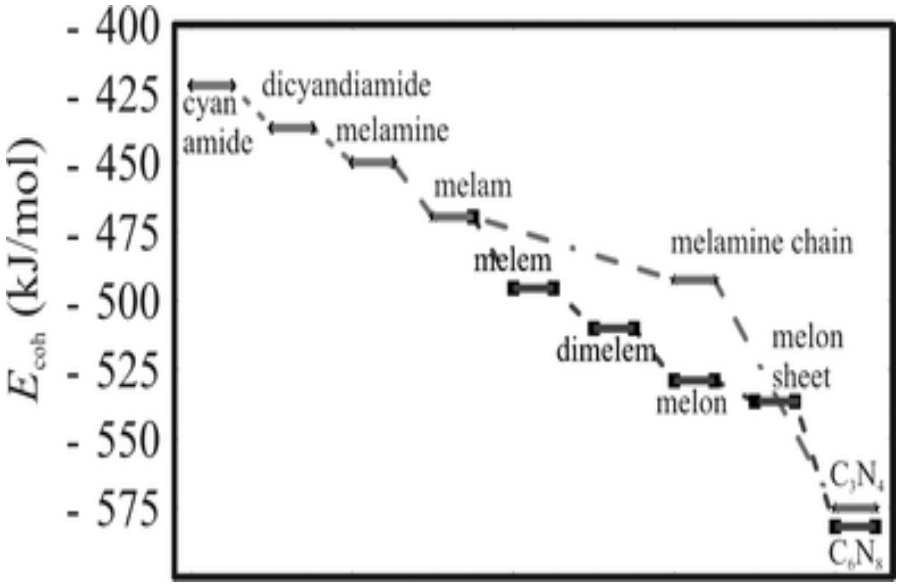

Fig. 1.6 Calculated energy diagram for the synthesis of carbon nitride. The energies are presented per atom. Reprinted with permission from Ref. [11] (License No. 1168038-1) Copyright@2008 The Royal Society of Chemistry.

A smaller number of reports are also available on postulated g-C_3N_4 structure based on triazine units, although it is thermodynamically less stable to the widely reported heptazine-based g-C_3N_4 structure. [4,12] One such report of stochiometric C_3N_4 linked with another triazine (C_3N_3) is of the carbon-nitrogen thin film prepared by thermal decomposition of chloro/fluoro trimethyl silane substituted C_3N_3 precursors ($C_3N_3F_2N(SiMe_3)_2$ and $C_3N_3Cl_2N(SiMe_3)_2$) in 1994. [13] A large crystalline thin film of triazine-based g-C_3N_4 was prepared interfacially at the gas-liquid interface reaction using dicyandiamide monomer and eutectic mixture of LiBr and KBr in ionothermal 2014 (*see* Fig. 1.4). It has a direct narrow bandgap of 1.6-2.0 eV of interest of electronic devices. [14,15] In the whole thesis, the term 'g-C_3N_4' refers to heptazine (or tri-s-triazine) based structure.

The carbon nitride nanosheets (CNNSs) possess extra merit to bulk CN material because of its higher surface area, greater number of surface-active sites, large band gap (credit to the quantum size effect) and enhanced e^- mobility along the in-plane direction. The CNNSs materials are of electronics and optoelectronics interest. The synthesis strategies of CNNSs are similar to the synthesis approach of graphene, the Bottom-up fabrication method and Top-down synthesis approach as depicted in Figure 1.7. The Top-down synthesis approaches include ultrasonication-assisted liquid exfoliation, post-thermal oxidation etching and a combination of these two techniques, while Bottom-up approaches are primarily Template-assisted synthesis, Heteroatom-mediated synthesis and Additive-mediated synthesis. [16] Both synthesis strategies yield CNNSs of the desired function. The obtained carbon nitride structure is composed of graphite-like stacks with close to hexagonal order within layers.

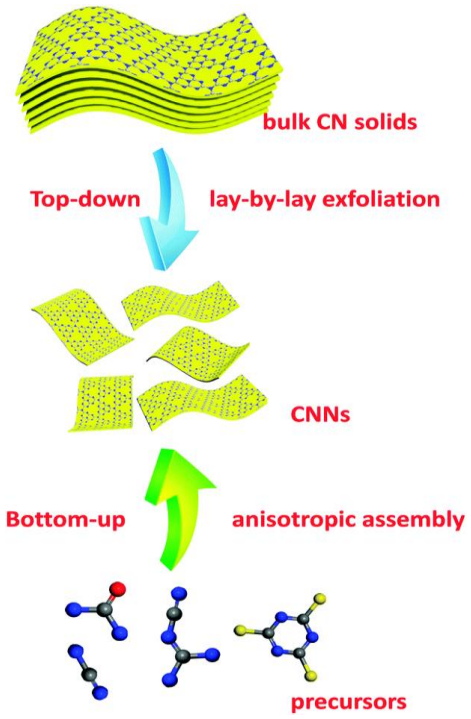

Fig. 1.7 The top-down and bottom-up synthesis strategies for carbon nitride nanosheets (CNNSs). Reprinted with permission from Ref. [16] (License No. 1168038-1) Copyright@2015 The Royal Society of Chemistry.

Graphitic carbon nitride term is also referred to those C_xN_y or CN materials with a sp^2 network of C and N atoms exhibiting the features of g-C_3N_4. This C_xN_y term is applicable for non-stoichiometric ratios (not 3:4 as in case of C_3N_4) of sp^2 hybridized constituting elements carbon and nitrogen, where used precursors are not conventional melamine or Urea as in the case of g-C_3N_4 synthesis, rather other N rich sources such as Cysteine, citric acid, sodium citrate, organic amines, formamide ($HCONH_2$) and substituted dimethylformamide (DMF). [17-23] Synthesis of these carbon nitrides (CN) materials is done by low-temperature heating or microwave treatment of single

or different molar ratios of two components in solid-state or in aqueous/organic media which gives zero dimension highly fluorescent quantum dots used for optical sensing and imaging application.

In some literature, the term graphitic carbon nitride (CN) is used for the materials synthesized via copolymerizing a mixture of conventional precursors viz. melamine, urea, dicyandiamide and a small amount of conjugated organic monomer to get an optimized morphology, optical and electrical properties. [24-28] Conjugated organic species viz. barbituric acid, oxamides, cyanuric acid, benzaldehyde, 2-Aminobenzonitrile (ABN), etc. have such functional groups that help them for easy integration into carbon nitride polymer and provide extended pi conjugation with enhanced separation of charge carriers. A range of amino and cyano groups bearing organic monomers are a great choice proposed for the functionalization of g-C_3N_4. [29]

1.2 Structural, Optical and Morphological Features

Graphitic carbon nitride (g-C_3N_4) has a polymeric two-dimensional structure that is strongly stacked together by van-der-Waal force as in the case of graphite. The as-synthesized bulk g-C_3N_4 has a yellowish powder appearance and a low specific surface area of 10-15 m^2/g. Use of different precursors viz. Dicyandiamide, Melamine and Urea, yields g-C_3N_4 of different crystallinity and (low) surface areas. The difference in the volume for the same weight amount of g-C_3N_4 prepared from two different precursors urea and melamine in our research lab can be easily seen in Figure 1.8. g-C_3N_4 synthesized at various target temperatures (viz. 450, 500, 550 and 600 ºC) using

precursor urea exhibits an increase in crystallinity and specific surface area with an increase of heating temperature.

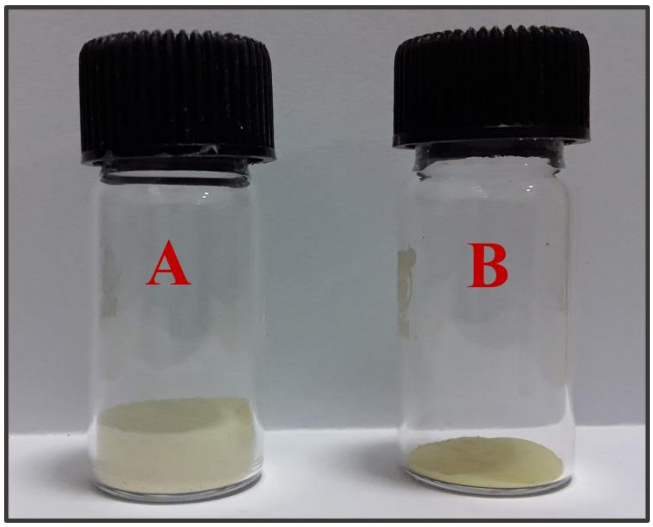

Fig. 1.8 Same weight amount of g-C_3N_4 prepared from two different precursors. (Difference in volume for same weight amount is easily visible.)

Unlike graphite, g-C_3N_4 has good wettability in H_2O owing to amino group at edges, which helps in easy dispersion in aqueous media and further breakdown into nanosheets (carbon nitride nanosheets: CNNSs) under continuous sonication. g-C_3N_4 are highly stable in acidic and basic media and hydrothermal treatment over prolonged time period show only increase of surface area value and no change in chemical identity. [16, 30-32]

1.2.1 Structural Features of Bulk g-C_3N_4

Figure 1.9 (a) exhibits the XRD pattern of the bulk g-C_3N_4 prepared using Melamine, one major peak along with one smaller peak has been indexed. Structurally, there is the in-plane repetition of tri-s-triazine units at 6.81 Å (equal to the distance of nitride pore) which features as characteristics 2θ peak at 13.0 º in XRD spectrum of g-C_3N_4. This dimension of 6.81 Å is smaller to the size of one tri-s-triazine unit (~7.13 Å), it is attributed to small tilt angularity in the graphitic structure (*see* Fig. 1.9 b). The conjugated aromatic system is stacked by van der Waals forces at interplaner spacing (d) of 3.26 Å appearing as a strong XRD 2θ peak at 27.4º. [33] This stacking distance is lower than the stacking of carbon in graphene (d = 3.53 Å) and more dense (~ 3 %) to the crystalline graphite. [34]

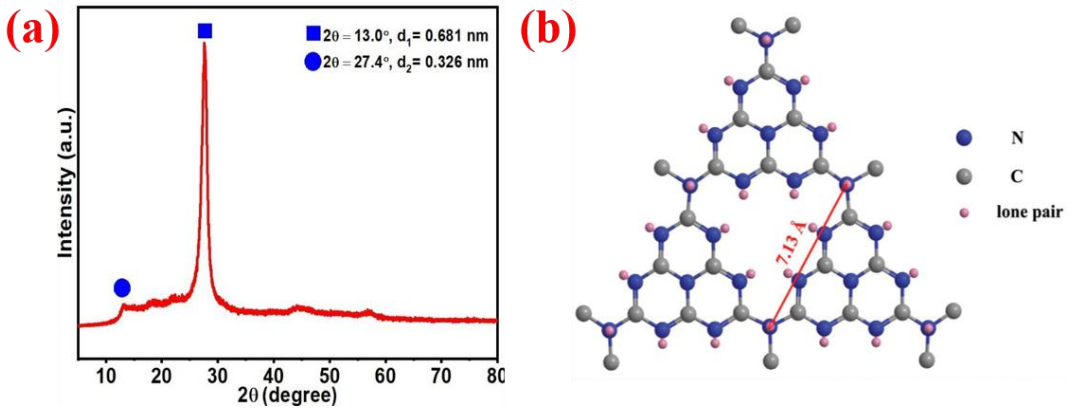

Fig. 1.9 (a) XRD pattern of the polymeric carbon nitride, revealing a graphitic structure with 3.26 Å of an interplanar stacking distance for aromatic units and 1.9 (b) the distance from one nitride pore to another nitride pore (size of one tri-s-triazine unit).

Carbon nitride sheets are stacked so strongly by van-der-Waal force that nanosheets of g-C_3N_4 show negligible shift in the position of $2\theta = 27^{o}$ with some loss of crystallinity in terms of reduction in peak intensity. Elemental analysis shows an average carbon-nitrogen (C:N) ratio of 0.72, while the theoretical ratio for C_3N_4 is 0.75. A very small amount of hydrogen (~ 2%) is also confirmed, contributed to the uncondensed amino group.

1.2.2 Optical Features of g-C_3N_4 and Band Gap

The UV-vis absorption edge of g-C_3N_4 prepared in the lab lies at 460 nm to the blue region of the visible spectrum, a typical absorption pattern of semi-conductor (see Fig. 1.10 a). The optical bandgap of the material was calculated from the Tauc method, further developed by Davis and Mott, using the following equation

$$\alpha h\nu = B(h\nu - E_g)^{n/2} \quad \text{..... (Eq. 1.1)}$$

where 'α' is the absorption coefficient, '*h'* is the Planck's constant, 'ν' is frequency, 'B' is a constant and 'E_g' is bandgap energy in electron volt (eV). The value 'n' depends on the kind of electron transition. For g-C_3N_4, an indirect transition, the value of n is 4. The optical band gap obtained from the corresponding Tauc plot (Fig. 1.10 (b)) is ~2.7 eV (E_{cb} = -1.3 eV; E_{vb} = +1.4 eV) which puts it into intrinsic semiconductor category. Since E (H_2O/O_2) requires 1.23 eV only, this band gap is sufficient enough to overcome the endothermic barrier of the water splitting reaction. Utilizing this suitable positioning of band gap and band alignment theory with other semiconductors, lots of

research work has been done to explore the photocatalytic water splitting features (viz. HER and OER) of g-C_3N_4 based composites materials. [27,35]

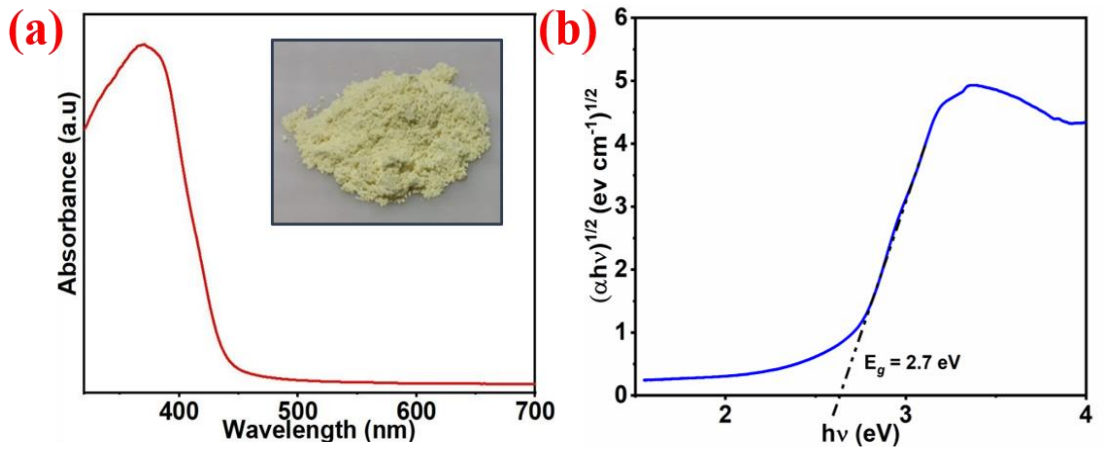

Fig. 1.10 (a) Ultraviolet-visible diffuse reflectance spectrum of the polymeric carbon nitride. Inset is the g-C_3N_4 prepared at 550 °C in our lab and Fig. 1.10 (b) shows the corresponding Tauc plot.

1.2.3 Morphological Features of g-C_3N_4 and Dimensionality

The yellow powdered g-C_3N_4 can be obtained in various kinds of morphologies such as sheets, spheres, tubes, wires and even in zero-dimensional quantum dots form using template synthesis method, top-down and bottom-up strategy.

As per the International Union of Pure and Applied Chemistry (IUPAC) categorization, there are three kinds of materials based on their average pore diameters: microporous (pore diameter < 2nm), mesoporous (pore diameter 2-50 nm) and

macroporous (pore diameters > 50nm). [36] For all catalytic (photo or electrocatalytic) and charge storage performance, a high surface area of material is desirous. Microporous materials provide a larger surface area via molecular sieving and diffusion effects. Although not always the high surface area of material is catalytically active or has accessibility to electrolyte ions, hence morphology, dimensionality and texture of material is also needed to be tuned to achieve higher performance. 2D structure with high aspect ratios provides a short ion-transfer path, while porosity prevents the overlapping and restacking of layers, hence access to interfacial sites.

Controlled heating of precursors viz. cyanamide, dicyandiamide, melamine in alumina crucible covered with lid in muffle furnace yield layered 3D graphitic structure of a low surface area. Use of silica nanoparticles, SBA-15 as a hard template, and Pluronic P123 as a soft template, a 3D structure of porous g-C_3N_4 with a high surface area is obtained. [37-39] A similar strategy is adopted for the synthesis of hollow g-C_3N_4 spheres as reported by Sun et al. [40] One-dimensional g-C_3N_4 nanostructure exists as nanowires, nanotubes, nanobelts and by controlling their length, diameter and aspect ratios, their electronic and optical properties can be tuned. The Zero dimension of carbon nitride (CN) viz. carbon nitride quantum dots (CNQDs) are generally prepared from non-conventional precursors using the bottom-up approach, it yields both stochiometric and non-stochiometric CN dots as reported in literatures. [17-23] One of our thesis chapters (Chapter 5) contains the synthesis of doped non-stochiometric CN dots and utilized its optical properties for the sensitive detection of carcinogenic pollutants. The synthesis approach of two-dimensional CNNSs is already discussed earlier in section 1.1.

1.3 Carbon Composites and g-C_3N_4 as Substitute of N Doped Carbon

Carbon materials exclusively graphene and carbon nanotube (CNT) are of great importance since possess a large surface area and excellent thermal, electrical and mechanical attributes. Modification of carbon materials with non-metallic elements viz. Boron, Nitrogen, Oxygen, Phosphorous greatly enhance their catalytic features by change of the electronic properties. [41,42] In N-doped carbon materials, integration of N into its carbon neighbors (mostly MWCNTs, SWCNTs, mesoporous carbon, graphene) as graphitic N, pyridinic N, pyrrolic N, and quaternary N (*see* Fig. 1.11) helps to overcome the limitation of carbon material by increasing the density of catalytic active sites and altering the electronic properties. Hard template method (using silica template), carbonization at higher temperature, chemical vapor deposition (CVD) is some of the techniques adopted in the preparation of N-doped carbon (referred as NC). [42,43] However, the relatively low N content (2-5 at. %) acts as a barrier to harness the full potential of prepared material under an extreme electrochemical environment. Graphitic carbon nitride has high nitrogen content (C/N=0.75) mostly in form of graphitic and pyridinic nitrogen, after modification and functionalization, this g-C_3N_4 serves as a substitute of N doped carbon materials (e.g., N doped graphene and N doped CNTs) in many electrocatalytic reactions and charge storage purposes. [44-46]

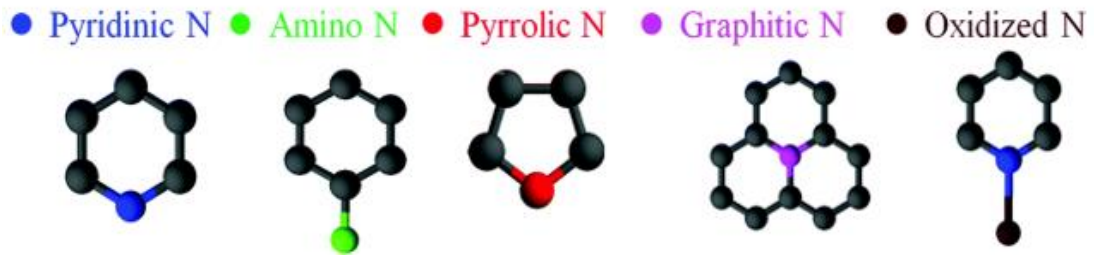

Fig. 1.11 Different bonding states of nitrogen atoms into the carbon (graphene) atmosphere. Reprinted with permission from Ref. [46] (License ID 1173032-1) Copyright@2021 The Royal Society of Chemistry.

1.4 Potential Application Area of g-C_3N_4 and its Composites

Carbon nitride is composed of two elements i.e., Carbon and Nitrogen, both earth-abundant elements, its synthesis step is low cost and properties are easily tunable by simple strategies without change in the overall compositions. Its band (Valence band and conduction band) positions, band gap value as well as inherent nitrogen in the carbon framework have allowed the researchers to explore its application' dimensions in both photo to electrochemical domains. The polymeric nature and wettability of g-C_3N_4 permits us to do surface chemistry using inorganic nanoparticles and other conducting polymers. As discussed earlier, the great importance of this material to advocate the energy and environmental concerns, the list of its potential application areas as heterostructures/hybrids is as follow

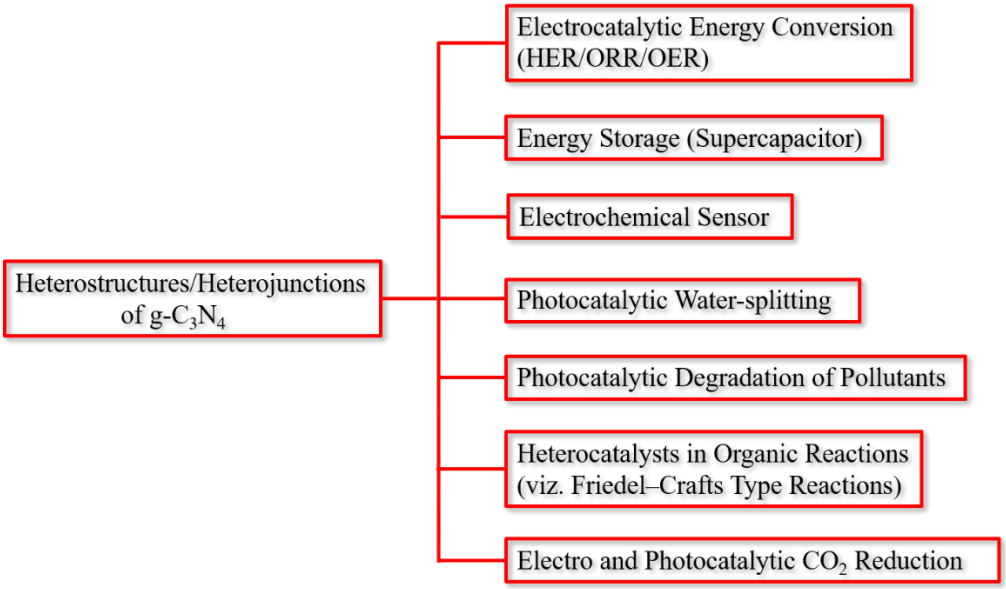

Fig. 1.12 Schematic illustration of the applications domains of g-C_3N_4 based heterostructure/hybrids.

g-C_3N_4 and its composites have proved as a substitute of precious metal-based electrocatalysts for energy conversion (viz. HER, OER and ORR) and have come out as a promising candidate for commercial carbon-based materials for energy storage. [33, 47] The semi-conducting nature and optical features of graphitic carbon nitride have led its exploration in many photocatalytic activities, and also as Heterocatalysts in organic reactions. g-C_3N_4 was firstly used in the heterogeneous catalysis field by direct activation of benzene in Friedel-Crafts reactions by F. Goettmann et al. in 2006. [48]

1.4.1 Limitation of Bulk g-C_3N_4 for Practical Application

Generally, carbon nitride (bulk g-C_3N_4) prepared from the N-rich precursors viz. Urea, Cyanamide, dicyanamide, melamine, is not suitable as such for electro or photo application, since it's as-prepared structure owes certain limitations. It has a small surface area (10-15 m^2/g), low conductivity and fast recombination of photogenerated e^--h^+ pairs limiting its use as a single candidate. For application into the nano world, a high specific surface area with greater porosity is desirous, so that any surface modification and functionalization can be easily performed to exposed sites. Advancement of technology and chemical knowledge has provided multiple avenues to tame these shortcomings of bulk g-C_3N_4 for practical application. Ultrasonic dispersion technique, acid treatment, hard-soft template methods, chemical functionalization are the tools to tailor the surface's physical-chemical features, mesoporous characteristics as well as electronic properties of the bulk material. Functionalization of g-C_3N_4 with other inorganic semiconductors, metals, conducting polymers, carbon materials and by doping with heteroatoms pave the way to for the use of this material in diversified fields.

1.4.2 Functionalization of g-C_3N_4: Heterostructures/Heterojunctions

Functionalization of g-C_3N_4 is required for enhancing its catalytic efficiency and further broadening its task-specific application dimensions. Disinfection, ECL detection, ferromagnetism, NADH generation and bioimaging are carbon nitride's new emerging application areas in addition to its electro and photocatalytic features

discussed in section 1.4. The various functionalization techniques for g-C_3N_4 for desirable properties with the specific application can be described in schematic illustration as follow

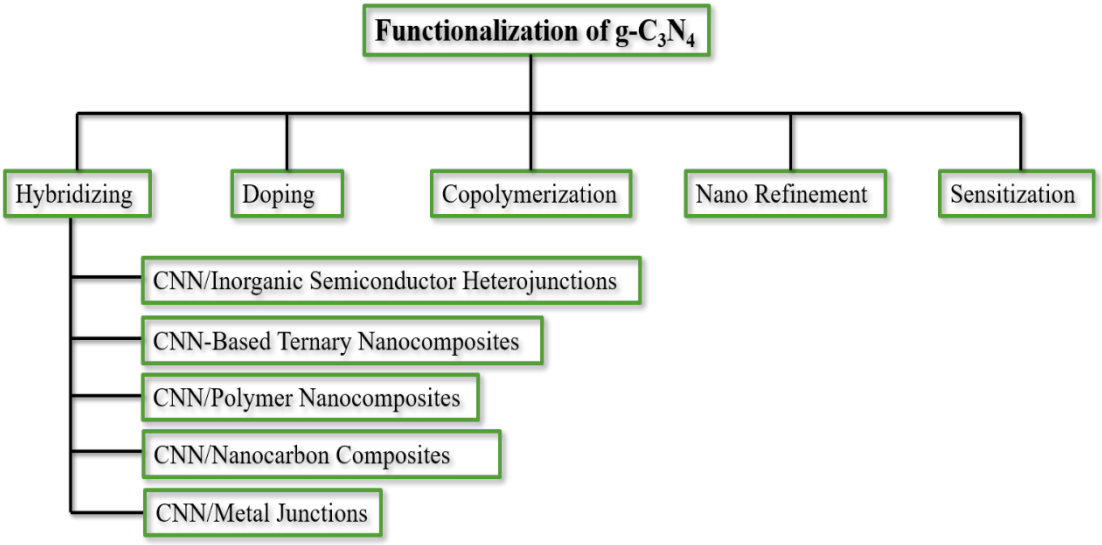

Fig. 1.13 Schematic illustration of the various functionalization techniques deployed for the carbon nitride for the task-specific application.

Among these techniques, hybridizing (or heterostructure formation) and doping methods are extensively used in our whole research work. We prepared g-C_3N_4 based ternary nanocomposites as well as iron carbide carbon composites and explored them for photo and electrocatalytic application. Henceforth, I will discuss the hydrogen energy, electrochemical water splitting phenomenon, 'Figure of the Merits' for an electrocatalyst, attributes of g-C_3N_4 and carbon-based materials for charge storage and

its evaluation parameters followed by photocatalytic and sensing features of g-C_3N_4'composites in brief.

1.4.3 Renewable Energy and Role of g-C_3N_4 as an Electrocatalyst

Clean and renewable energy is making a big share in overall energy profiles and global policy is more uphill to make Renewables available to every household. India is among one of those countries with the highest rate of growth for renewable energy (R.E.) in the world. Globally, India stands fourth in R.E. power capacity, 4rth in wind and 5th in solar power capacity. [49,50]

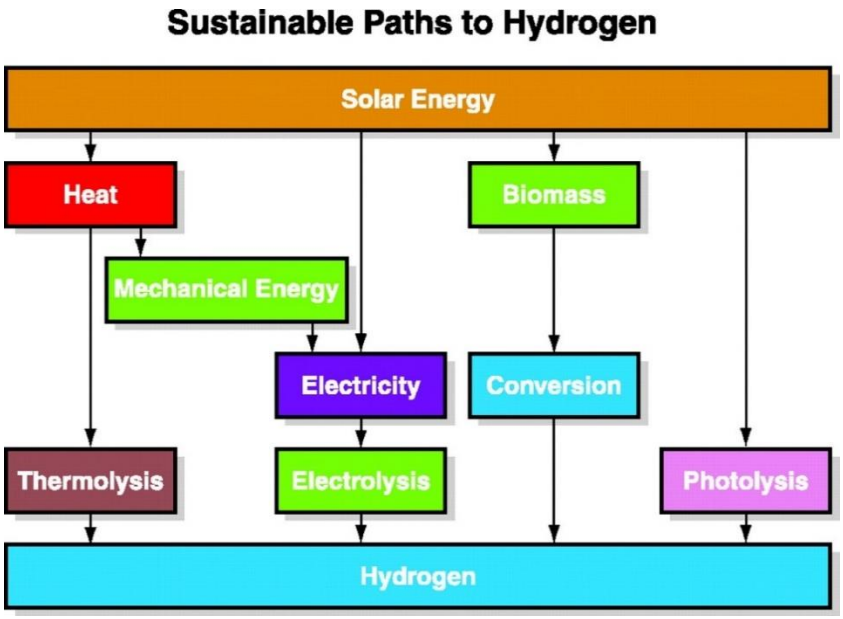

Fig. 1.14 Sustainable pathways from solar energy to Hydrogen (H_2). [51]

Among the various class of energy, the energy obtained from sunlight is paying big dividends to full fill the need. H_2 generation by water electrolysis driven by renewable electricity comes under sustainable production because of its source water being abundant and green hydrogen source (also *see* Fig. 1.14).

An electrocatalyst is required to help to drive the sluggish water-splitting process for a better outcome. Noble metal Platinum is still the most efficient electrocatalyst for it. Hence, the development of efficient non-Noble metal and earth-abundant element based electrocatalysts are highly desirous to reduce dependency on Pt-based materials and cost-effective H_2 generation. g-C_3N_4 in conjugation with other carbon materials and non-metal elements has served the purpose of electrochemical splitting of water as a low-cost electrocatalyst.

1.4.3.1 Hydrogen (H_2) as an Energy Carrier

Hydrogen as an energy vector, for storing and transporting energy, has served the energy demand being clean and efficient fuel but it's cheap and efficient source has always remained on the lookout. Hydrogen (H_2) generation by electrochemical water splitting driven renewable source is the phenomenon of conversion of renewable energy into chemical energy.

Hydrogen has an energy content of 120–142 MJ kg^{-1} is a great energy carrier. The 500 billion cubic meters of H_2 is produced worldwide annually. Many technological advancements have been made for hydrogen production. The coal gasification, steam methane reforming and water electrolysis are three major ways of

H_2 production, of which the contribution of water electrolysis in H_2 generation is only 4%. [52-54] Major Utilization of this Hydrogen is in petroleum refining industries, for Ammonia production in fertilizers industries and chemicals. Hydrogen fuel powered vehicles, also called Fuel cell electric vehicle (FCEVs), have attracted automobile sectors for its better pollution control. Hence, a cost effective, earth abundant elements based electrocatalyst for hydrogen generation will assist to achieve sustainable hydrogen economy.

1.4.3.2 g-C_3N_4 and its Composites as HER Electrocatalyst

The electrochemical water splitting phenomenon was first discovered by Paets van Troostwijk and Deiman in 1789 and Pearson reported this to the Royal Society on February 2, 1797 (published in the Philosophical Transactions). [55-57]

The whole electrochemical splitting of water is seen as combination of two half-cell process: The hydrogen evolution reaction (HER) and the oxygen evolution reaction (OER). The total reaction is as follow

$$H_2O \leftrightarrow H_2 + ½\ O_2 \quad \ldots\ldots\ldots\ldots\ldots\ldots \quad \text{(Eq. 1.2)}$$

In acidic, basis and neutral media, the reaction pathways are as follow

In acidic media: at cathode $2H^+ + 2\ e^- \rightarrow H_2$

At anode: $H_2O \rightarrow 2H^+ + ½\ O_2 + 2e^-$

In Basic and neutral media: at cathode $2H_2O + 2e^- \rightarrow H_2 + 2OH^-$

At anode $2OH^- \rightarrow H_2O + ½\ O_2 + 2e^-$

The change of free energy (ΔG°) for the conversion of one water molecule into H_2 and O_2 is +237.2 kJ per mol of H_2 at standard temperature and pressure (STP). Some extra work (TΔS°) is also required for the expansion of the gas, hence enthalpy change (ΔH° = ΔG° + TΔS°) in the process is +286 kJ per mol of H_2. The conversion of this thermodynamic value into reversible electrochemical cell voltage, $\Delta E°_{rev,298}$ = 1.23 V is required for water splitting at 1atm.

In practice, the applied potential is higher than this theoretical reversible thermodynamic value of 1.23 V to drive the electrochemical water splitting. The excess potential required in addition to this 1.23 V is called overpotential (η) of an electrocatalyst, it is used to overcome the kinetic barrier imposed by high activation energy during the formation of the reaction intermediates at both electrode surface (η_a and η_c) and also to overcome some solution resistance and others (η_{other}). Hence, operational voltage (E_{op}) for water splitting is given as follow

$$E_{op} = 1.23\,V + \eta_a + \eta_c + \eta_{other} \quad \text{..... (Eq. 1.3)}$$

Obviously, by designing of good electrocatalyst and optimizing the electrochemical cell, 'E_{op}' can be minimized. An efficient electrocatalyst has a lower overpotential value. In an electrochemical process, the applied potential is expressed by the Nernst equation as follow

$$E = E^o + \frac{RT}{nF}\ln\frac{[O]}{[R]} \quad \text{.....(Eq. 1.4)}$$

Where, various parameters have conventional meaning, [O] and [R] are concentrations of oxidizing and reducing agents, respectively. Now, overpotential (η)

can be given as difference of applied potential (E) and potential under equilibrium (E_{eq}) i.e.,

$$\eta = E - E_{eq} \qquad \text{..... (Eq. 1.5)}$$

1.4.3.3 Figures of Merit for Electrocatalyst

The Catalytic activity of an HER electrocatalyst is measured on some important kinetic parameters, can also be called 'Figures of Merit' described as follow

1.4.3.3 (a) Onset Potential and Over Potential

The activity of a catalyst as an electrode material is measured in terms of steady-state current, catalyst shows at a particular applied potential for a time slot. Output current is usually normalized with respect to geometrical electrode area (Amp cm^{-2}) or per unit mass (Amp g^{-1}). The Cyclic voltammetry (CV) or linear sweep voltammetry (LSV) technique is used for this estimation.

Onset potential is the potential, where the catalytic process begins, although there is no straightforward point/potential where one can deduce the beginning of the process, hence we assume onset potential is the point/applied potential, where a significant current density either 0.5 or 1 or 2 m Amp cm^{-2} should be observed.

Similarly, overpotential is that potential value, where a significant current density usually 10 m Amp cm^{-2} (refers as j_{10}) (current density required for 12.3 % solar water-splitting device) can be obtained. Both onset potential and overpotential are commonly used terms for electrocatalysts for comparison of their catalytic activities.

1.4.3.3 (b) Exchange Current Density (j_0)

It is an important parameter for electrocatalyst and indicator of electrocatalytic kinetics. In a water-splitting phenomenon catalyzed by an electrocatalyst, the total current is the sum of cathodic (i_a) and anodic (i_c) contributions.

$$i = i_a + i_c \text{ ……..……(Eq. 1.6)}$$

This cathodic and anodic contribution can further be elaborated as follow

$$i_a = nFk_a[R] \exp\left(\frac{\alpha_a nFE}{RT}\right)\text{……(Eq. 1.7)}$$

$$i_c = nFk_c[O] \exp\left(-\frac{\alpha_c nFE}{RT}\right)\text{……..……(Eq. 1.8)}$$

'k' and 'α' are rate constants of the cathodic/anodic half-reaction and cathodic/anodic transfer coefficient, respectively. At equilibrium, η = 0 and applied potential (E) becomes equal to equilibrium potential (E_{eq}), under such conditions, net current is zero and, cathodic and anodic currents are equal to each other i.e., $i_a = i_c$. The magnitude of i_a (or i_c) at equilibrium when η = 0 is called exchange current (i_0), when divide by the geometrical area of the electrode, is called as 'exchange current density' (j_0) as follow

$$\frac{i_0}{A} = j_0\text{……..……(Eq. 1.9)}$$

The magnitude of 'j_0' talks about the charge transfer and bonding at the interface of electrocatalyst and reactant. A high value of 'j_0' refers to a good electrocatalyst. Pt has the highest 'j_0' among gold (Au), rhodium (Rh) and Iridium (Ir), hence also exhibits superior catalytic activity to others.

1.4.3.3 (c) Tafel Equation and Tafel Slope

Current density (j) and overpotential (η) are related to each other according to the following well-known Butler-Volmer equation

$$j = j_0 \left[exp\left(\frac{\alpha_a\, nFE}{RT}\right) + exp\ \left(\frac{\alpha_c\, nFE}{RT}\right)\right] \ldots\ldots\ldots\ldots\ldots \text{(Eq. 1.10)}$$

Under the condition of high anodic/cathodic overpotential, the contribution from another part becomes negligible and the Butler-Volmer equation can be simplified into

$$j \approx j_0 \left[exp\left(\frac{\alpha_{c/a}\, nFE}{RT}\right)\right] \quad \ldots\ldots\ldots\ldots\ldots\ldots\ldots \text{(Eq. 1.11)}$$

This equation (Eq. 1.11) is also known as the **Tafel equation**. Further translation into logarithm function, the equation 1.11 can be re-written as

$$\log(j) = \log(j_0) + \frac{\eta}{b} \quad \ldots\ldots\ldots\ldots\ldots\ldots\ldots \text{(Eq. 1.12)}$$

$$b = \frac{\delta\eta}{\delta \log(j)} = \frac{2.303\ RT}{\alpha F} \ldots\ldots\ldots\ldots\ldots\ldots\ldots\ldots \text{(Eq. 1.13)}$$

Here, the term 'b' is the Tafel slope, it is elucidated from the graph of overpotential (η) vs logarithm of current density (j). Tafel slope measures how much overpotential is required for every ten-fold increase in current density and is usually given in mV per decade. Obviously, a smaller Tafel slope qualifies a catalyst to be good or ideal.

High exchange current density and small Tafel slope are two very important parameters for a good catalyst. Platinum exhibits a high exchange current density of

10^{-3} Amp cm^{-2} while, a low Tafel slope of 30 mV dec^{-1} considered among all reported electrocatalysts till now best.

1.4.3.3 (d) Gibbs Free Energy of Adsorption and Volcano Plot

Since all catalytic phenomenon takes place by the adsorption of molecular species on the electrode or catalytic surface, evaluation of Gibbs free energy of adsorption (ΔG_{ads}) serves as an important criterion to draw a comparison between various catalyst working for a fixed purpose. For HER electrocatalysts, Figure 1.15 represents the experimentally measured 'j_0' as a function of the DFT-calculated Gibbs free energy of adsorbed atomic hydrogen (ΔG_{H^*}). This plot depicts a Volcano shape with Pt metal at the top of the volcano having the highest 'j_0' and ΔG_{ads} close to zero.

Hence, an ideal catalyst should exhibit Gibbs free energy of hydrogen adsorption (ΔG_{H^*}) zero or near to zero. Edge site MoS_2 has shown modest ΔG_{H^*} and decent j_0 values. [58-60] Current density also depends on catalyst loading and the density of active sites. Stability, Faradic efficiency and Turnover frequency (ToF) are other 'Figures of Merit' of an electrocatalyst to be discussed in brief as follow

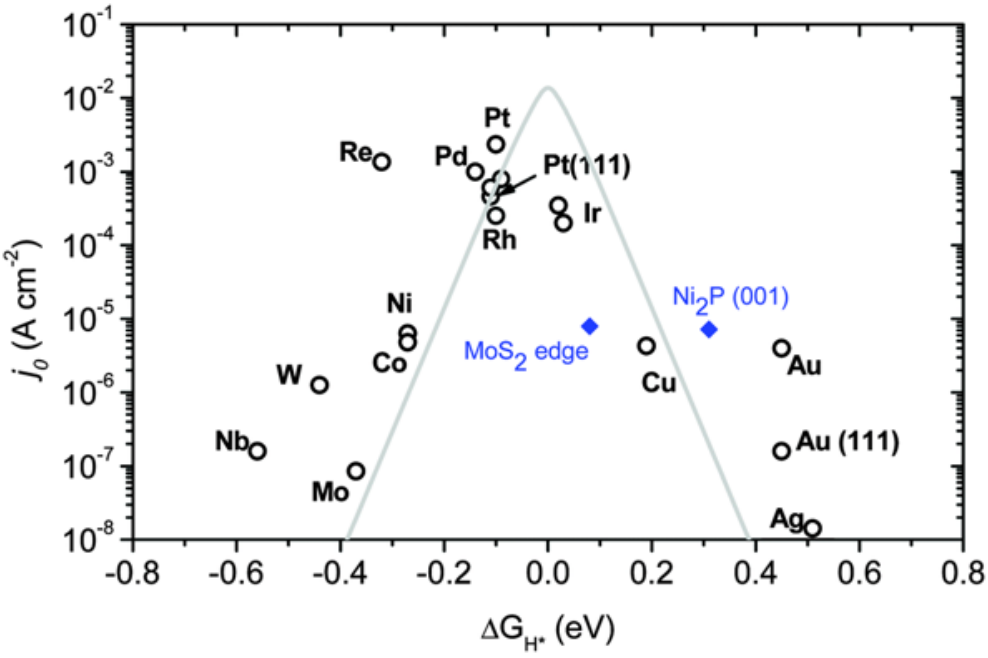

Fig. 1.15 A volcano plot of experimentally measured exchange current density as a function of the DFT-calculated Gibbs free energy of adsorbed atomic hydrogen. Reprinted with permission from Ref. [60] (License ID 1173365-1) Copyright@2014 The Royal Society of Chemistry.

1.4.3.3 (e) Stability

Electrocatalytic stability is measured with respect to time, generally, an overpotential value (for j > 10 m Amp cm^{-2}) is given for a longer period of time (say 12 h, 24 h, etc.) and % change in current density is measured. In another method, a large number of CV cycles is performed and change is current density is measured by LSV after the end of CV cycles.

1.4.3.3 (f) Faradic Efficiency

Faradic efficiency (F.E.) is the measure of an electron's efficiency to take participation in a redox process in the electrochemical system. Faradic efficiency is calculated as the ratio of experimentally H_2 produced and theoretical H_2 amount in case of an HER electrocatalyst,

1.4.3.3 (g) Turnover Frequency (ToF)

Turnover Frequency is the catalyst's ability to convert the reactants into product per catalytic site per unit of time. Although, it is hard to calculate the number of accessible active sites, hence ToF is not always precise.

1.4.3.4 Mechanism of HER

Electrocatalytic hydrogen evolution reaction is a multistep process (*see* Fig. 1.16), in acidic solution, three reactions are supposed to dominate (1) discharge reaction, where hydronium cation (H_3O^+) acting as proton source couples with the electron present on electrode surface yielding surface-bound H-atom. In an alkaline solution, proton source is the water molecule. Now, this surface-bound H-atom combines with another surface-bound H-atom yielding H_2 i.e. (2) combination reaction or there is another pathway in which Hydronium ion couples with surface-bound H-atom in presence of another electron yielding H_2 i.e., ion + atom reactions. [60] It is the Tafel slope that determines whether combination reaction or ion + atom reaction is dominating into H_2 evolution. A Tafel slope value corresponding to 2.3RT/2F shows the combination reaction as a

rate-determining reaction, while a slope value of 4.6RT/3F corresponds to ion + atom reaction as a rate-determining reaction in an HER system. The Tafel slope has been derived from the Butler-Volmer equation for three limiting reactions. [61,62]

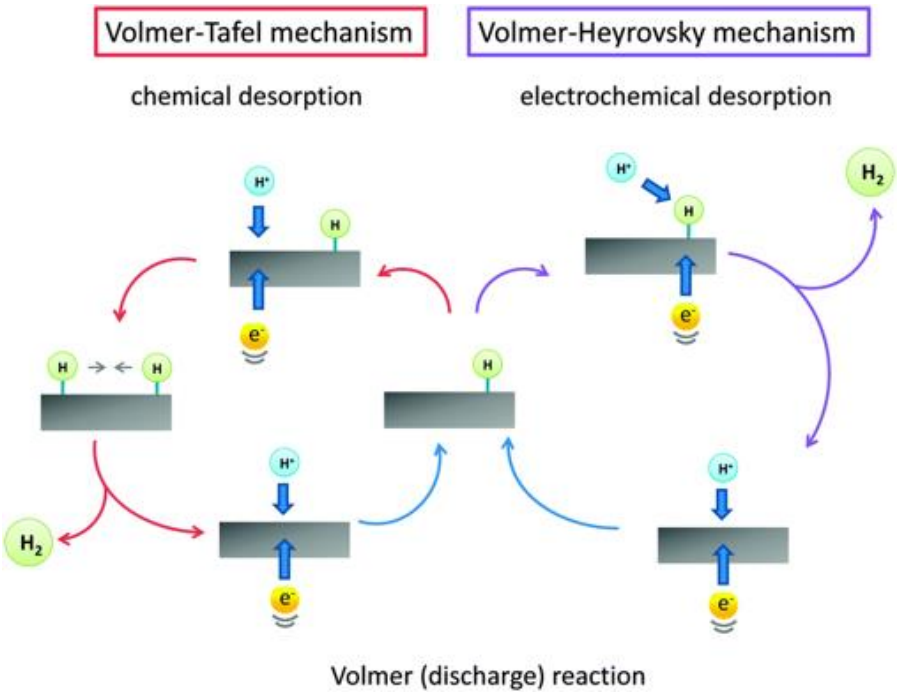

Fig. 1.16 The mechanism of hydrogen evolution on the surface of an electrode in acidic solutions. Reprinted with permission from Ref. [60] (License ID 1173365-1) Copyright@2014 The Royal Society of Chemistry.

1.4.3.5 OER and its Mechanism

Now, I will discuss another half of the water-splitting reaction i.e., OER taking place at the anode. OER is another important energy conversion process taking place in the system viz. fuel cells, alkaline water electrolysis, and metal-air batteries. RuO_2 and

IrO_2 are good OER catalysts, but besides being precious metals, they can easily oxidize at higher anodic potential, hence not suitable for large-scale practical applications. [64,65] Substantial research effort has been put to look out for the alternate, g-C_3N_4 as an alternative of precious metals has proved to be worthy along with other carbon compounds (Ti_3C_2, CNTs and graphene). [66,67]

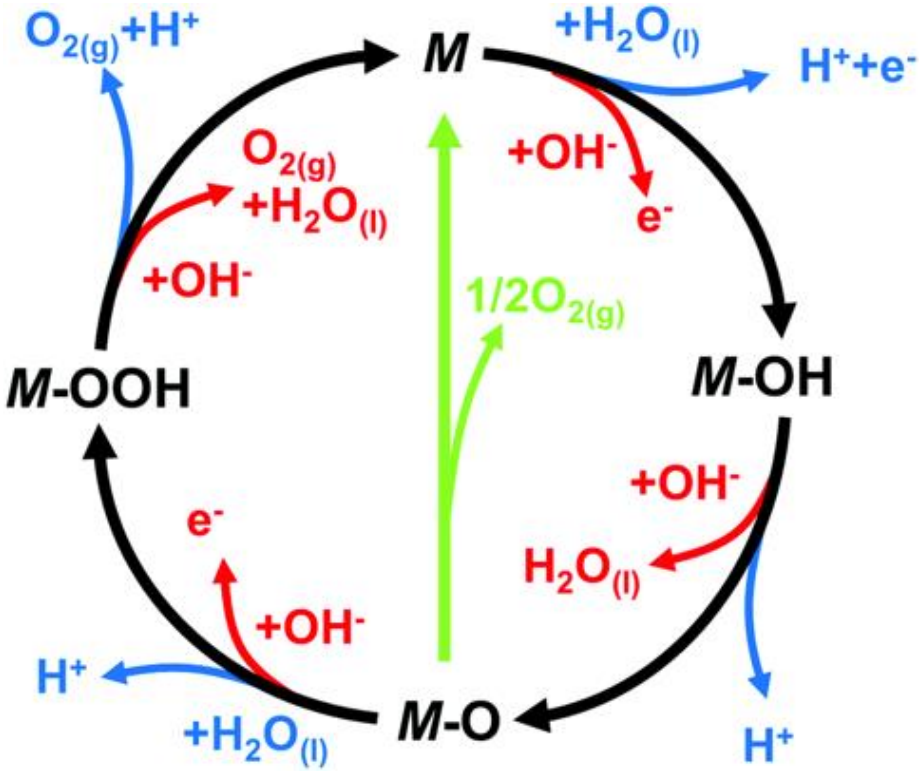

Fig. 1.17 The OER mechanism for acid (blue line) and alkaline (red line) conditions. Reprinted with permission from Ref. [63] (License ID 1173367-1) Copyright@2014 The Royal Society of Chemistry.

A flow diagram OER mechanism has been shown above in acid (blue) and alkaline (red) solutions in Figure 1.17. Electrocatalytic oxygen evolution reaction

(OER) is an anodic reaction and it involves a four-electron transfer process, hence it will require higher energy comparative to HER. It's a heterogeneous process and follows different pathways in acidic and basic media. In all proposed mechanisms, intermediates are the same i.e., MO, MOH and MOOH, the only difference that exists is the O_2 formation step. O_2 formation occurs either by direct combination of 2MO intermediates or decomposition of MOOH intermediate. In all phenomena, the interaction of chemical species to the metal surface is vital i.e., M-O interaction. Similar parameters exist to evaluate and compare different OER performing catalysts as mentioned in the above sections with a special focus on F.E. and ECASA.

1.4.3.6 Oxygen Reduction Reaction (ORR)

In proton exchange membrane fuel cell (PEMFC), oxygen reduction takes place by fusion of O_2 with protons and electrons resulting into water as product:

$$\frac{1}{2} O_2 + 2H^+ + 2e^- \rightarrow H_2O \quad \text{(Eq. 1.14)}$$

ORR is a cathodic reaction involving four electrons. It has very sluggish kinetics, which requires high loading of catalyst (~0.4 mg cm^{-2}) of Pt-based catalysts, hence hunt for alternate is on. g-C_3N_4 is a potential candidate for electrocatalytic ORR owing to high nitrogen content but suffers limitations in terms of poor conductivity and low surface area. Some recent research work done in the last decade has led to modification by the addition of rGO, GQD and MXenes which resultant in enhanced ORR performance. Co-metal coordinated g-C_3N_4 and carbon composites (Co-C_3N_4/C) exhibited dual activities in both ORR and OER. [68,69]

ORR study of an electrocatalyst is usually done by loading catalyst ink over the rotating disk electrode (RDE). Rotating disk electrodes enhance the mass transfer rate of O_2 at the surface of the electrode. This technique was introduced by Stonehart and Ross in 1976, later modified by Gloaguen et al. in 1994. [70] Koutecky-Levich equation (K.L. equ.) provides information about the intrinsic catalytic activity as follow

$$\frac{1}{j} = \frac{1}{j_k} + \frac{1}{j_{l,c}} = \frac{1}{j_k} + \frac{1}{0.62nFAC_0^* D_0^{2/3} \upsilon^{-1/6} \varpi^{1/2}} \ldots\ldots\ldots\ldots\text{(Eq. 1.15)}$$

Here, 'j' is measured current density, 'j_k' is kinetic current density and '$j_{l,c}$' stands for diffusion-limited current density, respectively. $J_{l,c}$ depends on a number of other factors viz. number of electrons participated (n), geometrical area of the electrode (A), Faraday constant (F), the concentration of the dissolved O_2 (C_0^*), the diffusion coefficient of O_2 (D_0), rotation speed of electrode (ϖ) and solution's kinetic viscosity (υ). K.L. equation is based on smooth electrode surfaces which follow theory of laminar flow. Determination of j_k is done by extrapolation from K.L. plot ($j^{-1/2}$ vs $\omega^{-1/2}$) at various rotation speeds.

1.4.4 Carbon Nitride as the Next Generation of Carbon-based Supercapacitors

Supercapacitors, also pronounced as electrochemical capacitors or ultra-capacitors, possess high power delivery capacity (>10 kW/kg) and can be charge-discharge in seconds. These have low energy density (~ 5 W h kg^{-1}), comparison to batteries (Li batteries can have 200 W h kg^{-1}). [71]

Supercapacitor works on fundamental principles of 'double layer capacitance' C_D popularly known as 'electrochemical double-layer capacitance (EDLC)' which is calculated as follows

$$C_D = \frac{\varepsilon A}{d} \text{ .....(Eq. 1.16)}$$

'ε' is dielectric constant, 'd' is separation distance (should be; ~Å) and 'A' stands electrode surface area (viz. large interfacial area). It does energy storage by charging of the 'double layer capacitance' by reversible ion adsorption at the surface of carbon material at the electrode/electrolyte interface. No redox reaction occurs in this process. Energy (W) and power (P) are two parameters for performance evaluation of supercapacitors, calculated as follows

$$W = \frac{1}{2\times3600} CV^2 \text{ and } P = \frac{V^2}{4R} \text{.....(Eq. 1.17)}$$

Here, 'V' is nominal voltage in volts and 'R' is series resistance. Both 'W' and 'P' are evaluated per unit weight or volume. The current research challenge is to enhance the energy density of capacitors to touch 10 W h kg-1 or more closer to batteries at a cheaper cost, which is linearly dependent on increasing capacitance value (C). Capacitance is tuned by the proper selection of electrode material which squarely affects the ion adsorption at the electrode/electrolyte interface.

Electrode materials, the major component of supercapacitors, have been widely researched to explore the best candidate. Among various electrode material options,

carbon-based supercapacitors (CSs) are widespread (80 % of commercial supercapacitors) owing to its natural abundance, high chemical stability and electrical conductivity, high surface area, broad operating temperature, a large number of charge-discharge cycles and high coulombic efficiency. However, activated carbon (AC) based CSs also have limited energy densities (< 10 W h kg^{-1}) into organic electrolytes, credit goes to slow mass diffusion and limited charge accumulation. [41,72] Structurally, CSs are made up of two electrodes (cathode/anode) dipped in the electrolyte (aqueous/nonaqueous) and an ion-permeable separator separating the two charge points.

Presence of heteroatoms viz. O, N, B, S and P in carbon materials enhance their volumetric performance (charge storage per volume). The addition of heteroatoms in carbon materials alters the donor-acceptor properties through its electron pair, driving surface faradic reaction providing addition pseudo capacitance. [73] Nitrogen as a dopant is a great choice for it besides increasing surface energy and reactivity. Nitrogen incorporation occurs in graphitic, pyridinic, pyrrolic, amino and oxidized forms. (*see* Fig. 1.11) N doping in carbonaceous structure is achieved either through post-treatment strategies such as CVD or in-situ approach. [42,43] In-situ strategy is considered better as it makes N more intimate within the material and a more stable part of the structure.

The two-dimensional g-C_3N_4 has inherent high nitrogen content, great thermal and chemical stability, aromatic features, eco-friendliness and easy synthesis approach, which attracted the researcher's interest to explore it as a substitute of N doped carbon-based supercapacitors. Although, bulk g-C_3N_4 has a large number of N atoms to be redox-active non-graphitic, but low conductivity, low surface area and large band gap hinder its energy storage application and related fields. Certain structural modifications

of CN or composites/hybrid/doping with other metal oxides/ions/polymers are required to unleash its potential.

Nanostructured carbon nitrides such as tubes, wires, ribbons, spheres, sheets have exhibited greater efficiency for both electro and photo domains owing to the high specific surface area, hence greater exposure of sites and interaction. Tahir et al. exhibited morphology control synthesis of graphitic carbon nitride in form of tubular g-C_3N_4 and g-C_3N_4 nanofibers (GCNNFs) as supercapacitor electrode exhibiting C_S value of 233.00 F g^{-1} and 263.75 F g^{-1}, respectively. [74,75] Composites of g-C_3N_4 with various nanostructured carbon materials, transition metal oxides and hydroxides, doping of metal/non-metal, metal sulfide, conducting polymers and metal organic framework (MOF) have also resultant in enhancement in specific capacitance (C_S) credit to the synergism of constituents. [47]

We have deployed this available literature knowledge to enhance the charge storage properties of g-C_3N_4 by structural modification as well as with different alkali metal doping. The positive outcome of the modification is described in our '**Appendix B**' along with results obtained and their interpretation.

1.4.4 (a) Role of Different Bonding State of Nitrogen in Catalytic Activity

Nitrogen as heteroatom is integrated into carbon materials in different binding states viz. pyridinic, amino, pyrrolic, graphitic and oxidized form as depicted in Fig. 1.11, generally through post-synthesis of carbon materials or by in-situ methods. [46] g-C_3N_4 carries its own nitrogen from precursor molecules in form of graphitic, quaternary (both within the sheets) and amino group at edges. Insertion of nitrogen into carbon

surroundings enhances the charge carrier density by the contribution of p-orbital electrons of N into the π-electron system of graphene or carbon materials. Nitrogen enhances the wettability of the electrode material and the number of available active sites, significantly changing the electrochemical performance of the catalyst. It was observed that N doped carbon has greater HER activity in acidic solution compared to alkaline, as reported by Long et al. [80] Activity of different bonding states of nitrogen has been put into the order as follow: pyridinic ≈ amino > pyrrolic > graphitic order for the electrocatalytic activity. This order can be justified by the change in the electronic environment brought by different bonding species of nitrogen. X-ray photoelectron (XPS) technique helps to quantify the relative % of various bonding states of N by deconvoluting the high-resolution nitrogen peak.

1.4.4 (b) Electrolyte Selection in Energy Conversion and Energy Storage

Suitable selection of electrolytes is also an important criterion in electrochemical analysis, which entirely depends on electrolyte constituents and stable operational potential window. Aqueous electrolytes viz. KOH, H_2SO_4 are the most common choices due to the small diameter of the ion and great conductivity (much higher to non-aqueous media), but operational only in the narrow potential window (< 1.23 V) because of water hydrolysis. Neutral aqueous electrolytes viz. Na_2SO_4, Li_2SO_4 overpass this potential window of 1.23 volt. Addition of redox-active pairs viz. I^-/I_3^-, $Fe(CN)_6^{3-}/Fe(CN)_6^{4-}$, hydroquinone/quinone as electrolyte additives provide pseudo capacitance with greater operational window. [41] Besides these, WIS electrolytes (super concentrated salt solution), Organic electrolytes (viz. TBAP in acetonitrile; TEABF4 in ACN/PC), ionic liquid electrolyte (operational window > 3 V) and (Quasi-

) solid-state electrolytes are other runner ups explored for electrochemical purpose and energy storage overcoming the short comes of aqueous one.

1.4.5 g-C_3N_4 as a Photocatalyst Material

Photocatalytic properties of g-C_3N_4 as a metal-free conjugated polymeric semiconductor were first discovered by Wang et al. in 2008 by its photocatalytic hydrogen evolution ability (published in N. Material). [33] Although the obtained quantum efficiency for the Pt-modified g-C_3N_4 was very low (~0.1% for $\boldsymbol{\lambda}$ = 420-460 nm), but this work opened new avenues of photocatalytic H_2 production by functionalization of g-C_3N_4 among the plethora of other inorganic semiconductors. [77-79]

1.4.5.1 g-C_3N_4 for Photocatalytic Organic Dye Degradation

g-C_3N_4 being a semiconductor photocatalyst has been widely utilized as an effective and economic tool to deal with organic pollutants discharged from textiles industries. These organic species and their subsequent breakdown components are toxic in nature and mutagenic to aquatic flora and fauna. Chemically, organic dyes are the combination of the chromophore (causes dye color) and auxochrome (causes intensification of color). Chromophores are azo (—N=N—), nitro (—NO_2), carbonyl (—C=O), methine (—CH=) and quinoid group. Among them, azo dyes consist of 70 % by weight of all, Rhodamine B, Methyl orange, Congo red are the major ones.

Semiconductor metal oxides, especially TiO_2 and ZnO have come out as promising candidates owing to their stability, non-toxicity and low cost, but faster $e^-/h+$ recombination and shorter wavelength coverage act as limiting factors besides being a metal container. Research of past one and half decades has greatly explored g-C_3N_4 as a pollutant degrading agent, being easy synthesis from cheap precursors, UV-visible absorption edge around 440 nm, resistance to acid-base environment and non-metal, non-toxic characters. The amalgamation of g-C_3N_4 with suitable polymers, metal NPs and metal oxide/carbonates/halides/phosphates chosen by band gap engineering and adhesion with g-C_3N_4 has significantly enhanced its quantum efficiency by Z scheme heterojunction for a number of organic pollutants and aromatics investigated. [78,81, 82]

1.4.5.1 (a) Z-scheme Photocatalysis

The original idea of the Z scheme in all g-C_3N_4 based photocatalysts and related systems arises from the electron transfer pathway in plant photosynthesis involving photosystem PS I and PS II (P700 and P680 respectively) in two different spaces giving a ‘Z’ appearance to the pathway.

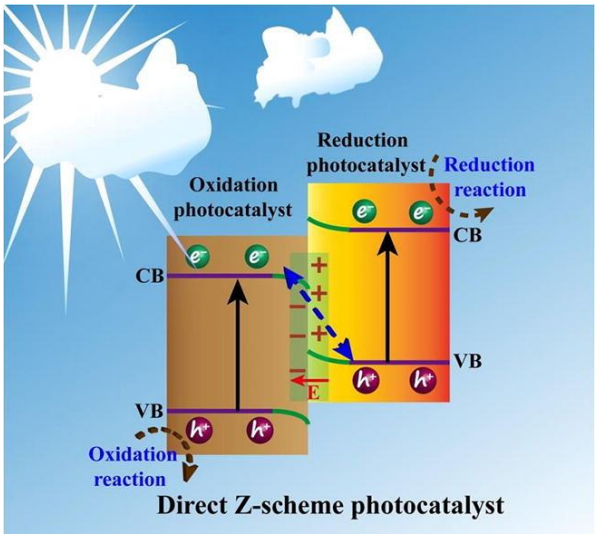

Fig. 1.18 Direct Z-scheme photocatalysts. Reprinted with permission from Ref. [81] (License Number 5221220341598) Copyright@2018 Elsevier.

In the photocatalytic dye degradation process, the main active species involved in breaking the dye are radical species viz. hydroxyl (˙OH) and superoxide anion ($\dot{O}_2^-$) radicals generated by oxidation of H_2O and reduction of dissolved O_2 respectively beside photogenerated charge carriers e^- and h+. Pure g-C_3N_4's E_{VB} (+1.4 eV vs SHE) falls lower to E(˙OH/H_2O) (+2.68 eV vs SHE), hence it could not oxidize H_2O to ˙OH resulting in lesser performance. The conduction band position of g-C_3N_4 (E_{CB} = -1.3 eV vs SHE) being lower to potential required for reduction of O_2 into $\dot{O}_2^-$ i.e., +0.13 (vs SHE) assist in catalytic activity, but quantum efficiency of pure g-C_3N_4 is not as good to be put into broader application. However, under the Z scheme heterojunction (*see* Fig. 1.18) such as TiO_2-g-C_3N_4 catalyst, effective separation of photogenerated charge carrier takes place leading to greater redox ability of photogenerated charge carriers e^- and h^+ respectively. [82]

A similar Z scheme heterojunction concept can be adopted for all g-C_3N_4 based solid-state composites to achieve excellent dye degradation results. These heterojunctions do not require any electron mediator that shuttles photogenerated electrons between two photocatalysts. Although, there is the optimum amount of either photocatalyst in heterojunction where it exhibits best photodegradation performance, further increase of either g-C_3N_4 or cocatalysts amount cause a negative impact on catalytic activity.

1.4.5.1 (b) Semiconductor Heterojunctions: Types

The binary or ternary heterostructures of g-C_3N_4 with another semiconductor co-catalyst chosen on band alignment promote longer separation of charge carriers at heterojunction interface. Classically, the band edges of two semi-conductors have one among three kinds of band alignments as depicted in Figure 1.19, Straddling (Type-I), staggered (Type-II) and broken (Type-III) gap. ΔE_C and ΔE_V are the band offsets of CB and VB, respectively. [76]

The band alignment creates space at the interface for charge accumulation and depletion promoting a longer lifetime of charge carriers.

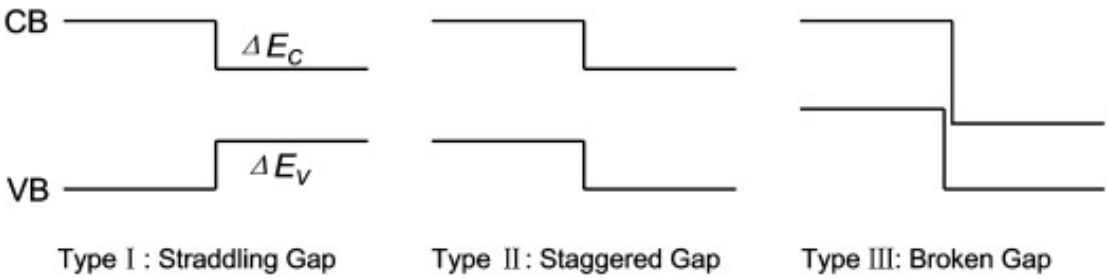

Fig. 1.19 Three kinds of semiconductor heterojunctions based on band alignment; Reprinted with permission from Ref. [27] (License Number 5250690259859) Copyright@2012 Wiley.

1.4.5.1 (c) Ternary Photocatalytic Heterostructures

Following the lineage of TiO_2-g-C_3N_4 heterojunction, a number of heterojunctions have been designed with the optimal combination of two or more metal oxide NPs addressed as binary or ternary systems resulting in enhanced photocatalytic activity. Such heterojunctions with NPs overcome the individual limitations of g-C_3N_4 along with the bonus of more stability and reusability. [83-89] The ternary heterostructure has the same electron transfer Z scheme, but it involves three separate catalysts in space.

1.4.5.2 g-C_3N_4 as Sensing Material

g-C_3N_4 has also been explored for its intrinsic peroxidase-like mimetic activity similar to carbon materials, due to its surface affinity for metal NPs viz. Au/Pt and single-stranded DNA (ssDNA). [90, 91] ssDNA adsorbed on g-C_3N_4 nanosheets has a four times faster reaction rate to g-C_3N_4 nanosheets alone for H_2O_2 mediated TMB oxidation. The interaction of carbon nitride nanosheets (CNNS) with fluorophore-labeled ssDNA is through nucleobases which led to fluorescence sensing of DNA and opened avenues for the application of 2D nanomaterials in bioanalysis.

1.4.5.2 (a) Fluorescent Sensing by CNQDs

Interaction of g-C_3N_4 with incident light can be optimized by controlling the dimensionality of g-C_3N_4. Carbon nitride when fabricated to zero-dimension scale is called quantum dots (CNQDs), it exhibits fluorescence properties that can be utilized for selective detection of many pollutant species to a high level of sensitivity. The

fluorescence properties of carbon nitride quantum dots are tunable with the size (diameter) of dots similar to carbon dots.

The fluorescence sensing technique is based on absorbance and is known for its simplicity, sensitivity and quick response time, unlike others sensing methods. Fluorescence is a phenomenon of photoluminescence, where material absorbs shorter wavelength (high energy) light and emits higher wavelength (low energy), mostly in the visible region. There is the singlet-to-singlet transition of electron (allowed transition) as per the well-known Jablonski diagram (*see* Fig. 1.20) from the excited state to any of the ground states, hence emission time is very short usually of ~10 ns. Florescence is non-radiative transition of electrons; it means electron goes from higher energy state to any nearest lower energy state without emission of photons.

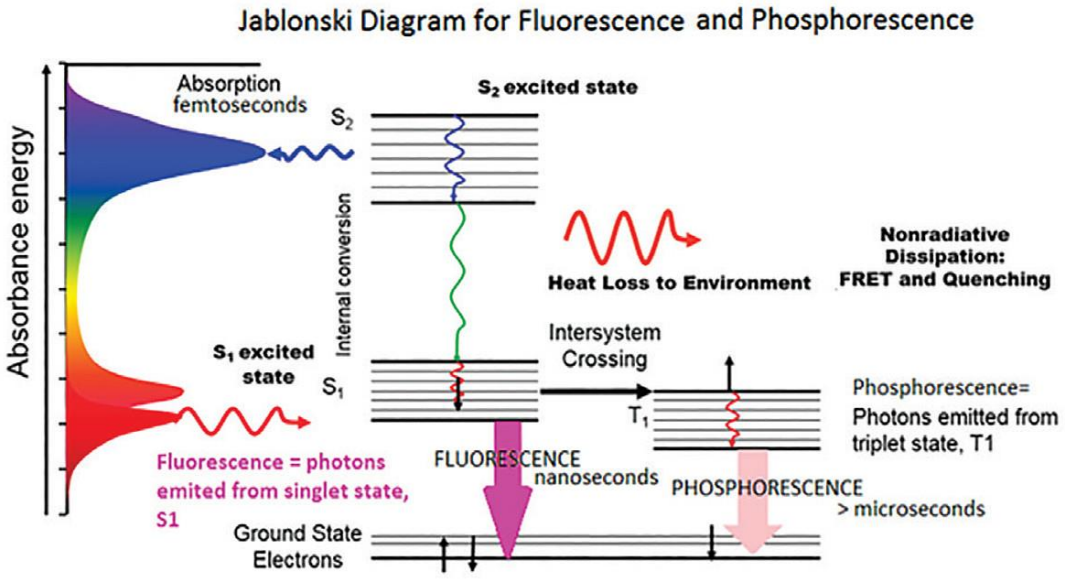

Fig. 1.20 Jablonski Diagram for Fluorescence and Phosphorescence. (Courtesy: Horiba.com)

In Phosphorescence, another category of photoluminescence, there is a singlet-triplet transition (forbidden transition) of electrons i.e., electrons having different multiplicity via intersystem crossing (ISC) while returning from the excited state to any of the ground states. Phosphorescence involved radiative transition due to dissipation of energy while returning to ground level.

1.4.5.2 (b) Life Time of Fluorescent Materials

Life time is the average delay time between excitation and emission of photons when interacting with a fluorescent material. For a fluorescent material, life time is of the order of 10^{-8} to 10^{-10} seconds. The average life time (τ_{avg}) of a population of fluorescent material is calculated as time in which 36.8 % of the excited species exponential decay to the original population of all excited species via the loss of energy (non-radiative process). This quantitative estimation of photoluminescent properties is called time-resolved PL (transient PL; TRPL). In the Case of Phosphorescence, life time is much larger of the order of 10^{-3} to 10 seconds, as some time is required for spin conversion of the electron when returning back to the ground state. The position of emission wavelength is always longer than the excitation wavelength due to energy loss either by radiative means or collisions with each-others, this shift of peak positions is called the ***Stokes shift***.

For studying the photoluminescent behavior of carbon nitride materials and quantum dots, we consider both Fluorescence and Phosphorescence to be included under photoluminescent (PL) or florescent terms used for carbon nitride in earlier reported works of literature and in our study. The distinction between these two is only

required when the emission life time of material is of the order of time constants of measuring instruments.

1.4.5.2 (c) Fluorescent Quantum Yield (Q.Y.)

Quantum Yields of florescent carbon nitride dots, graphene dots and other carbon dots are measured using the following equation with respect to quinine sulfate as standard (Q.Y. 0.54 at 360 nm)

$$QY_x = \mathrm{QY_{ref}} \frac{\mathrm{I_x\, A_{ref}\, \eta_x^2}}{\mathrm{I_{ref}\, A_x\, \eta_{ref}^2}} \qquad \text{……..……(Eq. 1.18)}$$

Where ‘QY’ stands for quantum yield, ‘I’ stands for integrated emission intensity, ‘A’ stands optical density and ‘η’ stands the refractive index. ‘X’ and ‘ref.’ stands for sample and reference, respectively.

Since the fluorescence phenomenon occurs by light interaction at the surface, the presence of charged groups (functional group) plays a pivotal role in initiating the PL process and hence the value of quantum yield. Surface functionalization of CNQDs, selection of suitable precursors and use of its optimal ratios in bottom-up synthesis approach are methods to optimize the fluorescence quantum yield of dots. [22,92]

1.4.5.2 (d) Limit of Detection (LOD)

Qualitatively, the Limit of Detection is the lowest concentration of analyte which can be reliably detected, while, quantitatively, it is three times of the standard deviation as follow

$$LoD = \frac{3 * SD}{m} \text{.....(Eq. 1.19)}$$

'SD' stands for standard deviation, while m refers to the slope of the linear fit line. LoD is the lowest value that can be statistically distinguished from a blank. The acceptable signal-to-noise ratio should be 3:1 or 5:1 (in some cases 10:1). it is used as a measure of the precision of the sensing method or technique. LOD value also refers to > 95 % probability of obtaining the correct value. [93]

Photoluminescent carbon nitride dots have been successfully deployed for colorimetric sensing of glucose and H_2O_2, dopamine sensing, Hydroquinone sensing, bio-imaging and other purposes. CN dots prepared using two or more precursors have been optimized for their emission properties and exhibits impressive quantum yield value. [17-23]

1.4.6 g-CN as Catalyst Support

Proton exchange membrane fuel cells (PEMFCs) (viz. hydrogen fuel cell, methanol fuel cell) have precious metal-based nanoparticle catalysts (ideal particle size ~ 3 nm) such as Pt nanoparticle deposited on catalyst support in effort of cost reduction of cell and catalyst support also maximize the ECASA of the NPs. [47] Commercial 'State-

of-the-art' catalyst support is carbon black having high surface area; however, it has its own disadvantage in terms of reduction in catalytic performance under repeated cycling and corrosion of cell chamber at the catalyst-support interface.

Among the wide range of tested catalyst supports, graphitic carbon nitride is at prime focus having a high concentration of N as part of its framework. N is known for its higher affinity to Pt NPs; hence it acts as a further stabilizer of catalyst by inhibiting agglomeration. Pyridinic nitrogen of carbon nitride forms charge transfer (CT) complexes with platinum and also enhances MOR and ORR activities. Although pure g-C_3N_4 is far from practical applications owing to poor conductivity (band gap of 2.7 eV) and lesser surface area, but in conjugation with conducting materials viz. graphene and non-Noble metal catalysts viz. Fe, Co, it serves the purpose of catalyst support, exhibits HER/ORR activities. [68] Hence, g-CN being an N framework better supports Pt and other nanoparticles with good dispersion and durability, decreases the catalyst loading and enhanced the overall catalytic performance. [94]

1.5 Scope of the Work and Objective of the Thesis

The quest in the field of renewable energy-based catalysts with care for the environment has put the emphasis for the development of such catalytic material with no precious metal in its composition. The literary descriptions reveal the semiconducting features of g-C_3N_4 with absorption edge in the visible range and inherited N present in its framework in higher ratio; these features have employed it in a range of applications with additional modifications particularly involved structural

and morphological alteration as in its hybrid compositions. Though, a wide space is yet to be explored. For instance, heterojunctions based photocatalyst using g-C_3N_4 as the primary component and optimizing the dimensionality to tune the optical features of carbon nitride has less availability of reports. In addition, the electrochemical phenomenon (water splitting and energy storage features) based on this material is no or less explored by the research community obviously due to low surface area and low conductivity. Therefore, we assimilated our research objectives based on the concepts of hybrid materials' formation having the expectations to reduce these issues. The hybrids of g-C_3N_4 with other non-metal elements viz. carbon structures, phosphorous can be studied for electrocatalytic properties in order to achieve the benchmark performance of other noble metals and other TMDCs e.g., MoS_2. Similarly, the availability of a number of semiconductors like metal oxides put the chance to be chosen as cocatalyst of g-C_3N_4 on the basis of band alignment. The optimum tuning of these heterojunctions gives an opportunity for greater utilization of incoming radiation for photochemical purposes. In addition, the light interacting properties of carbon nitride material can be tuned by controlling its dimension for sensing applications. Secondly, the carbon materials have been deployed in the electrochemical conversion(s) and storage field since many decades; however, the incorporation of metal carbide into carbon matrix has few reports in this area. Hence, another scope opens up here in order to find the alternatives of costly electrocatalysts. Apart from these, the selection of a suitable synthesis process is another optimized area in order to enhance the photochemical as well as electrochemical performance.

In view of the above scopes, the objectives of the present thesis are

- To prepare the heterostructures and hybrids of graphitic carbon nitride and carbon materials in order to enhance the photochemical as well as the electrochemical performance of the composite synergistically.
- Synthesis of desired hybrid materials by pyrolysis and hydrothermal approach as they are prompt to yield materials having high surface area and active sites.
- Incorporation of iron carbides in carbon matrix for energy conversion purposes.
- Doping of heteroatoms viz. S, O-atom into the hybrid materials by the choice of suitable precursors in order to enhance the active sites for electrochemical applications.
- Incorporation of doped quantum dots as one of the dimension tools in the carbon nitride for sensing of pollutants.
- Selection of semiconducting co-catalysts based on band alignments into hybrid material applied for dye degradation purposes.

The thesis primarily focuses on materials prepared by choosing the earth-abundant elements as hybrid structures and heterojunctions formation to investigate their potentials in related fields. The outcome is encouraging and interesting. The tests of photoresponsive materials are based on real samples that provide an insight in order to deploy them at a larger scale.